Nanoscale

COMMUNICATION

View Article Online
View Journal | View Issue

Cite this: *Nanoscale*, 2015, **7**, 6492

Received 11th December 2014,
Accepted 12th March 2015

DOI: 10.1039/c4nr07332k

www.rsc.org/nanoscale

Assembly of a tile-based multilayered DNA nanostructure†

Junyoung Son,‡[a] Junywe Lee,‡[a] Anshula Tandon,‡[a] Byeonghoon Kim,[a] Sanghyun Yoo,[a] Chang-Won Lee[b] and Sung Ha Park*[a]

The Watson–Crick complementarity of DNA is exploited to construct periodically patterned nanostructures, and we herein demonstrate tile-based three dimensional (3D) multilayered DNA nanostructures that incorporate two design strategies: vertical growth and horizontal layer stacking with substrate-assisted growth. To this end, we have designed a periodically holed double–double crossover (DDX) template that can be used to examine the growth of the multilayer structures in both the vertical and horizontal directions. For vertical growth, the traditional 2D double crossover (DX) DNA lattice is seeded and grown vertically from periodic holes in the DDX template. For horizontal stacking, the DDX layers are stacked by binding the connector tiles between each layer. Although both types of multilayers exhibited successful formation, the observations with an atomic force microscope indicated that the DDX layer growth achieved with the horizontal stacking approach could be considered to be slightly better relative to the vertical growth of the DX layers in terms of uniformity, layer size, and discreteness. In particular, the newly designed DDX template layer provided a parallel arrangement between each domain with substrate-assisted growth. This kind of layer arrangement suggests a possibility of using our design scheme in the construction of other periodic structures.

Introduction

For a few decades, DNA has been used to design a variety of artificial self-assembling nanostructures[1–5] since it has a remarkable ability for highly specific dimerization. DNA follows Watson–Crick base pairing and, relative to other biomolecules, has a striking binding specificity, high thermodynamic stability, and a double helix structure with high persistence. Advances in DNA assembly have allowed a wide range of 1D and 2D structures and patterns to be fabricated. However, the subsequent expansion into the fabrication of 3D DNA structures has been a challenge[6–11] due to obstacles related to the unspecific assembly and structural instability in the 3D design, particularly for tile-based DNA design schemes.

Recently a variety of assembly strategies have been developed to construct 3D DNA structures[12–14] as tools for bionanotechnology, structural analysis, algorithmic computations, molecular sensors, enzymatic cascades, drug delivery, tissue engineering, and device fabrication. Currently, a small number of 3D structures have been fabricated *via* tile-based DNA self-assembly by employing homogeneous motifs that bind to each other.[13–17] However, the recently developed substrate assisted growth (SAG) method has not yet been used to design any of such 3D nanostructures,[18–22] despite the fact that this method has been proved to be more efficient in growing a variety of dimensional nanostructures, such as rings, single strand tile-based ribbons, and DX lattices. In SAG, electrostatically charged substrates are used as catalysts to promote the growth of the tile-based DNA nanostructures.[18,20,23] Additionally, bulk 3D structures can also be fabricated by stacking 2D arrays to form highly regular inter-array multilayer structures that depend on the Mg^{2+} concentration.[24]

Here, we incorporate two design strategies, SAG and 2D parallel layer stacking, to demonstrate a compelling approach to construct different types of tile-based 3D multilayered DNA nanostructures. For the vertical growth of the multilayers, we initially constructed a DDX tile-based 2D layered DNA nanostructure using a mica assisted growth (MAG) method. The vertical growth of this nanostructure imparts it with an expected layer-to-layer distance of 6 nm. Consequently, we stack these vertically-grown structures upon each other in a horizontal manner by using a homogeneous linker motif. This horizontal layer stacking produces a uniform step height of 2 nm (duplex diameter), which corresponds to the original design strategy.

[a]*Department of Physics and Sungkyunkwan Advanced Institute of Nanotechnology (SAINT), Sungkyunkwan University, Suwon 440-746, Korea.*
E-mail: sunghapark@skku.edu
[b]*Samsung Advanced Institute of Technology (SAIT), Suwon 443-803, Korea*

†Electronic supplementary information (ESI) available: Schematic diagram for tiles forming -mono, -bi and -multilayers; strand and sticky end details of tiles used for -mono, -bi and -multilayer formation; AFM image and height profile of fully grown vertical DDX layer. See DOI: 10.1039/c4nr07332k

‡These authors contributed equally to the paper.

Experimental section

Multilayer design in the vertical and horizontal directions

As stated above, our experimental strategy involves constructing a layered 2D structure that can be used to stack multiple layers in the vertical and horizontal directions. For vertical growth, two types of DNA nanostructures were used. One structure is the template that acts as a base, and it anchors another structure that is composed of multiple layers grown from a seeding site on the template. In this regard, we designed a structure for use as a base template, named DDX, seen as T0 in Fig. 1(a). The motif consists of three duplexes; the outer two are short with 18 and 19 base pairs each, and the central third is relatively long with 69 base pairs. Each short duplex is linked to the central duplex in plane by crossover junctions, and these are separated by two full-turn-length B-form DNA. The motif has single-stranded cohesive overhangs at each end of the duplex, known as sticky ends. The two short duplexes have two different types of sticky ends, referred to as Sa4′, SA2 and SA2′, Sa1′, respectively, at each terminus according to the type of binding in which they are involved. The capital 'A' in the middle of SA# and the lower case 'a' in the middle of Sa# represent sticky-ends binding for the DDX template and for the layer binding, respectively. The central strand also consists of two sticky ends, SA1 and SA1′. These sticky ends can assemble with their complementary counterparts in a repetitive fashion along the 2D DDX plane direction of the DNA duplex. Once the DDX template has been formed, holes with an expected periodicity of 25.2 nm [Fig. 1(b)] are generated along the lines of the short duplexes depicted in the AFM image of Fig. 1(c). The value measured for the distance is 26.6 nm, which is in good agreement with the expected value. The area with a single hole formed by the DDX template has dimensions of 12×4 nm^2, which is equivalent to half of DX.[25]

The DX L1 and L2 motifs shown in Fig. 1(d) were chosen as the best candidates for the multilayer structure grown from the DDX template. The DX lattice is a tile-based 2D structure that consists of two DX tiles. Each tile consists of side-by-side double-stranded helices that are linked at two crossover junctions 16 bases apart. These DX motifs assemble to form a 2D layer *via* complementary sticky end base pairs, shown as Sa# and Sa#′ in Fig. 1(d). The DDX template with holes is assembled and has active binding sites with a DX motif (L1) of the same periodicity and length, enabling the insertion of DX motifs into the DDX holes. We used the angle control scheme to ensure that the DX layers had a proper orientation nearly perpendicular to the DDX template structure.[26] When the DX L1 motifs bind into the holes of the assembled DDX template, the base pair distance between the closest crossover junctions of the DDX and DX motifs is of 18 and 19 base pairs for either of the sides with ~103° angles, which is an inherent characteristic of B-form duplex DNA.[13,25,27] This controlled base pair distance ensures that the 2D DX structure grows from the DDX template.

For horizontal stacking, the DDX structure used as a template layer for vertical growth was planned for use in the main multilayered structures. For a bilayer design, two sticky ends at the 5′ end of the L2 motif (Sa1′ and Sa4′), which were previously complementary with the 5′ end of the L1 sticky ends (Sa1 and Sa4), were replaced by the same sticky ends as L1. These new sets of motifs were named Cb1 and Cb2, also called connector tiles, and this pair of Cb# motifs accommodates a second layer of the DDX structure instead of providing continuous vertical growth for the Cb1 and Cb2 motifs, which was the case for vertical growth. The bilayer design terminates the DDX structure stacking at the second layer, but the multilayer design does not have the specified number of stackings. In the previous DDX design for the vertical layer growth, all of the sticky ends at the DDX holes were designed for growth with one orientation, thus accommodating only one pair of DX motifs (L1 and L2). However, the DDX tile is modified into a two-tile DDX system, and two pairs of sticky end sets with two different orientations are encoded into the sticky ends of DDX, binding one more pair of a connector tile set. Here, by putting one pair of the sticky end set to 5′ (Sm1′ and Sm2′) and another set to 3′ end (Sm5′ and Sm6′) (Fig. S4 in ESI†) of the hole sites, the orientation of DX motifs flips by 180 degrees. This increase in the degree of complexity leads to a two-fold increase for the connector tile sets, with the Cm1 and Cm2 pair binding to the holes in the original direction and the Cm3 and Cm4 pair in a reversed direction.

DNA crystal fabrication

Synthetic oligonucleotides purified *via* high performance liquid chromatography were purchased from Bioneer (Daejeon, Korea). We annealed the DDX template both in solution [Fig. 1(b)] and on the mica substrate. Then, 2-step annealing followed to fabricate two different multilayered structures, *i.e.*, the DX multilayer on the DDX template and the DDX bilayer. A one pot annealing method was also used in order to obtain DDX multilayers [Fig. 2(h)].

Free solution annealing for DDX (T0), DX (L1 and L2), and DX connector (Cb1, Cb2, and Cm1–Cm4) tiles

100 nM of DDX template was formed by mixing a stoichiometric quantity of each strand in physiological buffer [1× TAE/Mg^{2+} (40 mM Tris, 20 mM acetic acid, 1 mM EDTA (pH 8.0), and 12.5 mM magnesium acetate)]. This T0 tile strand mixture was annealed, cooling down slowly from 95 to 25 °C by placing a test tube in a Styrofoam box containing 2 L of boiled water for 24 hours to facilitate hybridization. In the case of the DX and DX connector tiles, the concentration of the strands was adjusted to 200 nM.

Mica-assisted growth of DDX template

The mica-assisted DDX template was formed by mixing a stoichiometric quantity of each strand and a cleaved mica substrate (5×5 mm^2) in 1× TAE/Mg^{2+}. This mixture of T0 tile strands with the mica substrate was annealed in a test tube to slowly cool it down from 95 to 25 °C in a Styrofoam box containing 2 L of boiled water for 24 hours in order to facilitate selective hybridization.

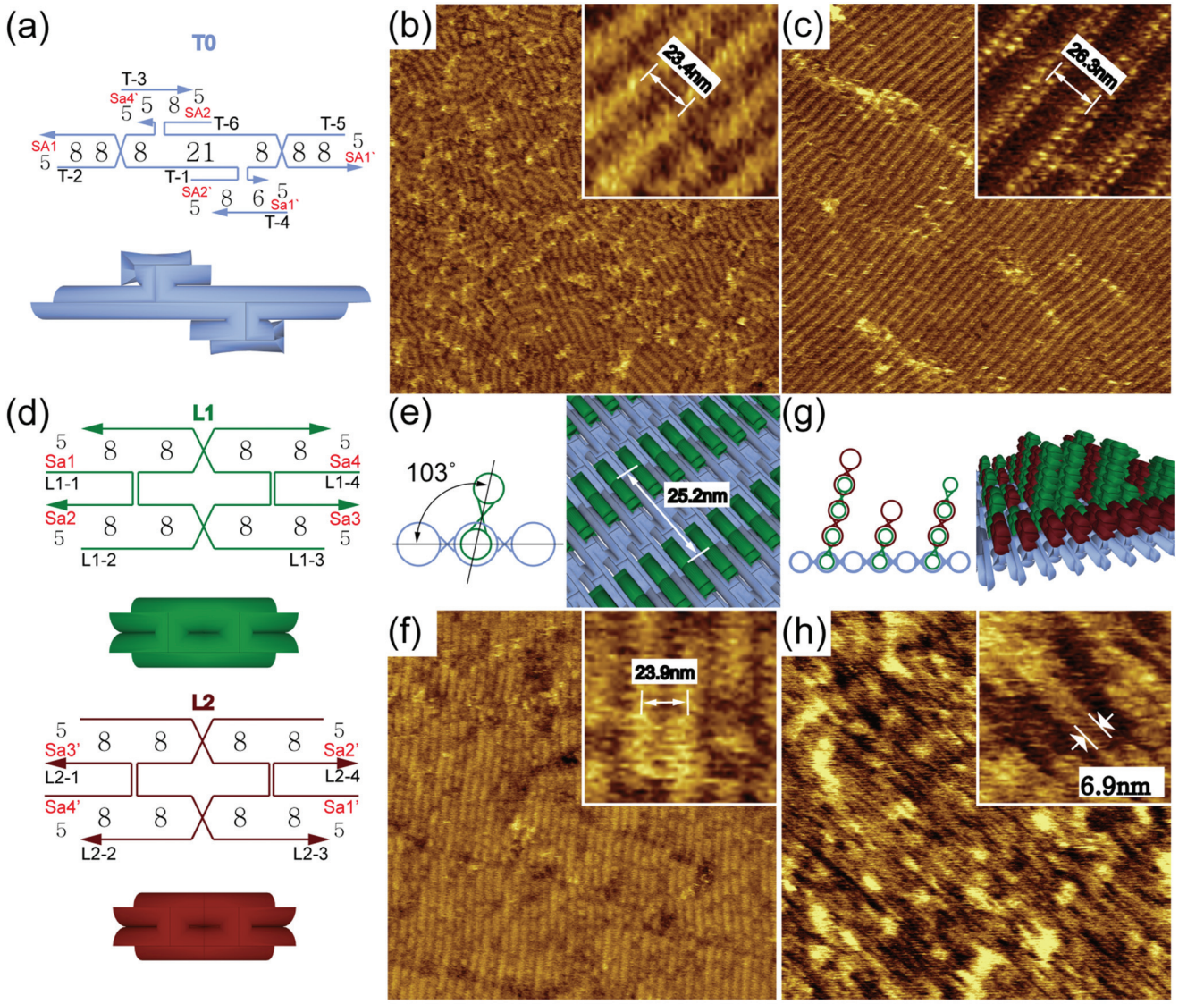

Fig. 1 Schematic design and AFM images of the double–double crossover (DDX) structure. (a) Schematic diagrams and 3D illustration for a DDX tile (T0) structure. Note that the capital 'A' in the middle of SA# and the lower case 'a' in the middle of Sa# represent the sticky-end bindings for template formation and for layer seeding sites, respectively. (b) The AFM images for the free-solution annealed assembly of the 200 nM DDX structure. The distance measured between the intermolecular junctions of DDX, represented as bright lines or as stripes, is of 23.4 nm, against an expected value of 25.4 nm. (c) DDX structure obtained *via* mica-assisted growth. The average stripe distance measured was of 26.3 nm. (d) Schematic diagram and 3D illustration of the double crossover (DX) tiles. (e) Side view and 3D illustration of the vertical binding of L1 into the self-assembled DDX structure. The blue circles represent the DDX (T0) template while the DX (L1) tile binding between Sa1′ and Sa4′ is shown with green circles. The addition of the L1 motif to the DDX template confers a 103° angle between the two structures with the expected distance between holes along the helical direction of the DNA being 25.2 nm. (f) The AFM image of the L1 tile bound to self-assembled DDX structure. The distance measured between the L1 junctions of the DX structure is approximately 23.9 nm. (g) Side view and 3D illustration for the growth of the L1, L2 multilayer structure on the DDX template. Here, the DDX (T0) and the DX (L1, L2) motifs are shown in blue, green, and red, respectively. (h) AFM image of the fully-grown multilayer DX structure on the DDX template with a distance between the layers of 6.9 nm (expected value of 6 nm). The scan sizes of the AFM images and their insets are 1 × 1 μm^2 and 100 × 100 nm^2, respectively.

Synthesis of the DX multilayer

2 μL of 200 nM L1 motif was dropped on the DDX template and incubated for 5 min to aid its binding to the DDX template [Fig. 1(e and f)]. In order to promote and observe a significant growth in the multilayered DX structures, we adopted a different method in which the DDX template was placed in a mixture of pre-annealed L1 and L2 motifs, and the mixture was then annealed in order to cool it down from 37 to 30 °C over 30 min [Fig. 1(g and h)].

Synthesis of the DDX bilayer and multilayer

In order to fabricate the DDX bilayer, the DDX template grown on mica was gently rinsed with 1× TAE/Mg^{2+} buffer solution

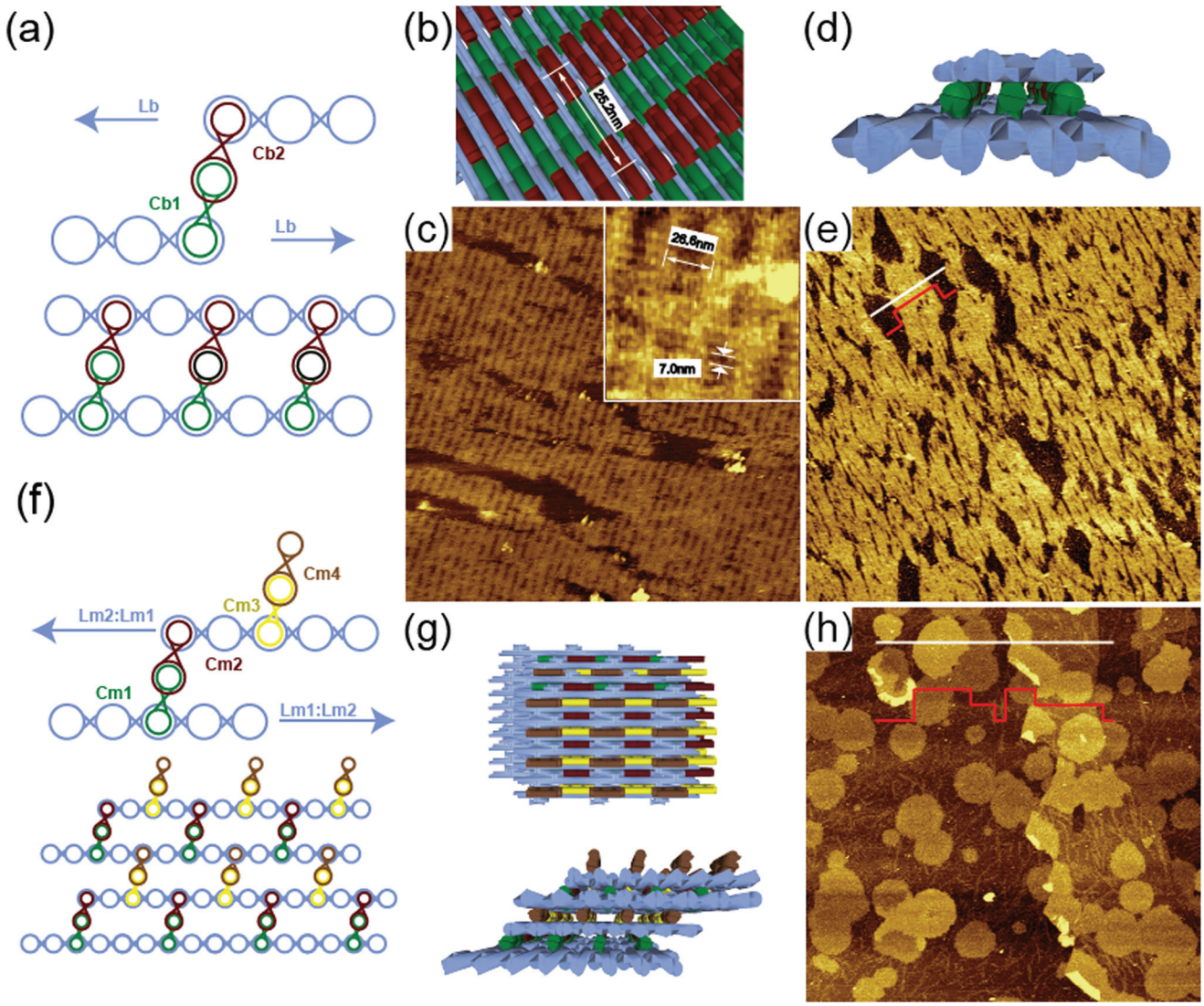

Fig. 2 Schematic design and AFM images for the stacked layer DDX structure. (a) The top part depicts the schematic design of the unit cell formed from the Lb, Cb1, and Cb2 motifs required for the bilayer assembly. The bottom shows the schematic design used to form the DDX bilayer by binding Cb1 and Cb2 with Lb. (b) 3D illustration depicting the arrangement of Cb1 and Cb2 on the DDX template prior to formation of the second layer. Here the DDX template and the Cb1 and Cb2 connectors are shown in blue, green and red, respectively. The distance expected between the junctions of the Cb2 motif of the DX structure is ~25.2 nm. (c) AFM images of the DDX template with Cb1 and Cb2 tiles attached to the respective binding sites. The distance measured between the intermolecular junctions, represented as stripes in the vertical direction, is 26.6 nm. The Cb1 and Cb2 motif rows in the helical direction of the DNA are indicated with narrow lines with a 7 nm periodicity. (d) 3D illustration of the DDX bilayer formed by binding the Cb1 and Cb2 covered by Lb motifs. (e) AFM image of the DDX bilayer structure formed from Lb, Cb1, and Cb2 motifs. The red line represents profile height along the cross section indicated by a white line. The step height distance is of ~2.2 nm. (f) Schematic design of the stacked multilayered DDX structure. The top depicts the design of the unit cell of multiple layers formed from Lm and Cm motifs. The arrows indicate the direction of the layer growth. The bottom shows a schematic design of the DDX multilayer formed by binding Cm1, Cm2, Lm1, and Lm2 motifs. (g) 3D cartoon depicting the mica-assisted growth assembly of the stacked multilayered DDX structure. The colour scheme is the same as in (f). (h) AFM image for the stacked multilayered DDX structure obtained from one pot annealing. The red line represents the height profiles along the cross section, as indicated by a white line. The step height distance is of approximately 1.2 nm. The scan size for all AFM images is $1 \times 1\ \mu m^2$ with an inset (c) of $100 \times 100\ nm^2$.

for a few seconds and was then placed sequentially into each test tube containing 200 nM of Cb1, Cb2, and DDX motifs. The sample was allowed to anneal for 20 min in Cb1 and Cb2 motifs and for 30 min in the DDX motif, cooling down linearly from 37 to 30 °C on a heat block. One-pot annealing was adopted to fabricate the 50 nM DDX multilayer where Cm1, Cm2, Cm3, and Cm4 strands as well as Lm1, Lm2 strands in a ratio of 1 : 2 were annealed together *via* MAG.

AFM imaging

For the AFM imaging, the DNA sample was placed on a metal puck using instant glue. Then, 30 μL of 1× TAE/Mg^{2+} buffer

was pipetted onto the substrate and another 20 μL of 1× TAE/Mg^{2+} buffer was dispensed into a silicon nitride AFM tip (Veeco Inc., USA). The AFM images were obtained with the use of a Multimode Nanoscope (Veeco Inc., USA) in the liquid tapping mode.

Results and discussion

Free-solution and MAG methods were both employed to assemble the DDX template. In the case of the MAG method, the strands that were required to form a DDX template were allowed to anneal on an atomically flat and electrostatically charged mica substrate. Mica acts as a catalyst and therefore reduces the cost of free-energy for seeding and crystallization of the DNA nanostructures, resulting in a larger crystal domain size as well as full coverage[18–21] when compared to crystals annealed in free solutions. The AFM images in Fig. 1(b and c) show that MAG is relatively better than free-solution annealing for DDX template fabrication in terms of the domain size and crystal arrangement. The images of the DDX templates annealed with both free-solution and MAG [Fig. 1(b and c)] show that the average stripe distances of 23.5 ± 2.4 nm after analysing 45 distances and 26.3 ± 1.4 nm after analysing 110, do not deviate much from the inter-junction distance of 25.3 nm of the design, which indicates that the structure was fabricated as designed in both cases. However, the size of crystal domains *via* MAG is noticeably larger than that of the free-solution method by more than 3 times, and the alignment of each domain is nearly parallel in the case of the MAG method. In free solution, the orientation of each domain within a scan size of 1 × 1 μm^2 is random. The sizes of the vertically grown DX multilayers and the horizontally stacked DDX layers are dependent on the size of the DDX template. Consequently, we employed MAG for further experiments.

The binding of the L1 motif into the holes in the DDX template was tested by comparing the AFM images before and after dropping 2 μL of L1 motif onto the DDX template. This L1 motif has complementary sticky ends with holes in the DDX template [Sa1, Sa4 and Sa1′, Sa4′ shown in Fig. 1(a and d), respectively]. Fig. 1(f) shows the AFM image for the L1 + DDX complex. Interestingly, the lines for the bilinear dots representing two intra-molecular junctions in T0 [inset in Fig. 1(c)] are no longer visible after adding the L1 motif, and instead, bold and wide stripes of the same distance are observed as bilinear dots. This is an indication of the L1 motif being bound into the DDX structures. To see the full growth of the DX multilayers, two-step annealing was adopted. A pre-annealed DDX template was put in a test tube containing L1 and L2 motifs, and the test tube was placed on a heat block with temperature decreasing from 37 to 30 °C over 30 min.

Since each side of the L1 sticky ends is complementary to the other side of the L2 sticky ends (Sa2, Sa3 & Sa2′, Sa3′ and Sa1′, Sa4′ & Sa1, Sa4, see Fig. S1 in ESI†), the mixture of L1, L2, and DDX template forms multilayered structures *via* self-assembly [Fig. 1(g)]. Fig. 1(h) shows an AFM image viewed from the top of the DX multilayers fully grown vertically from the DDX template after the completion of the annealing process. A stripe with an average distance of 6.9 nm can be observed, and the periodicity of the narrower distance is not shown in the previous structure, in accordance with a predicted value of 6 nm of spacing between the layers. After the DX layers are grown upward, periodic 26.5 nm stripes become inconspicuous as a result of the depth of the DX multilayers. Despite the little evidence of the DX multilayers in the DDX template, it was difficult to determine the height of the DX multilayers due to the complete DDX coverage on the mica substrate. However, AFM images with a relatively large scan size of 30 × 30 μm^2 occasionally produced a few trenched areas with a depth of ~25 nm, which had apparently formed as a consequence of the DDX template flipping on mica initially and thereby suppressing the binding of the initial L1 motif into the hole. This led us to postulate that the DX multilayers could grow to an average height of ~25 nm, which is obvious from the AFM image that is made of vertically grown DX multilayers (see Fig. S2 in ESI†).

Although the experimental results of the vertical growth for the DX multilayers provided reasonably good evidence of multilayered structures, there are certain limitations in controlling the height of DX layers. In contrast, horizontal growth uses the DDX template as a layer and the modified DX motifs as connector tiles. This provides a clear picture of the layer growth, as compared to the case with vertical growth. Fig. 2(c) shows the AFM image of the DDX (Lb) + connector tiles (Cb1 + Cb2) complex before adding DDX (Lb) for the second layers (see synthesis of DDX bilayer and multilayer in the Experimental section). Bright lines with a 26.6 nm distance for the inter-molecular junctions along the duplex are visible as well as fine lines with a ~7 nm distance for the connector tiles perpendicular to the duplex, as shown in the inset of Fig. 2(c). The width of the bright line is measured to be 13.7 nm, which is close to the length of the DX motif (12.5 nm). After the second layers form by adding a DDX motif (Lb) on a previously prepared DDX + connector tiles complex, the stripe patterns (bright and fine lines mentioned earlier) are no longer visible and a step height difference of about 2.2 nm can be observed, as indicated by the red line in Fig. 2(e), which confirms that the bilayer structure has formed.

Besides the DDX bilayers, we designed stacked DDX multilayers. The design of the stacked DDX multilayers is shown in Fig. 2(g) where all DNA tile sequences are designed to be unique from each other. The AFM image [Fig. 2(h)] shows circular island-like multilayers with a step height of ~1.2 nm between the stacked layers. Although the motifs that assemble the layered structure are sequentially controlled with two-step annealing in the DDX bilayer structures, this stacked multilayered DDX engages all strands at once during annealing. Therefore, full coverage of layer-by-layer assembly is hardly achievable. Instead, localized and piled layers can be seen in the structures of the AFM image [Fig. 2(h)]. The height profile analysis of these stacked islands for the DDX multilayers [red line in Fig. 2(h)] based on the cross section of the white line

shows a step height difference of ~1.2 nm, which corresponds to the diameter of duplex DNA on the charged substrate. The reason behind the formation of these circular layers is not clear, but we assume that the different annealing procedures (two-step and one-pot) could produce these changes in the topology.

Conclusions

In summary, we have constructed tile-based multilayered DNA nanostructures using vertical growth and horizontal layer stacking with the aid of the substrate-assisted growth method and an angle control scheme. We designed double–double crossover nanostructures with periodic holes that served as either scaffolds for multilayer growth or as layers on a given substrate. Consequently, multilayer growth in both the vertical and horizontal directions could be easily controlled using the proposed method, and AFM images revealed that the multilayered DNA nanostructures had good agreement with the expected geometries. Various kinds of novel and intriguing layer arrangements based on our design scheme can be used as a platform for generating highly periodic arrays of functionalized nanomaterials. The proposed method may also prove to be relevant for self-assembly of tile-based periodic multilayered lattices that make use of other types of tiles, such as a cross tile[28] or a 3-point star motif.[29]

Acknowledgements

We thank Jihoon Shin and Bong Gyu Shin for helpful discussion. This work was supported by the SAIT-SKKU Joint Research Fund, Samsung Electronics Co. Ltd, 2012 (IO120331-00909-01) and by the National Research Foundation of Korea (NRF), funded by the Ministry of Science, ICT & Future Planning (MSIP) of the Korean government (NRF-2012M3A7B4049801, NRF-2012-R1A2A2A01005985, and NRF-2014R1A2A1A11053213).

Notes and references

1 N. C. Seeman, *Nature*, 2003, **421**, 427–431.
2 N. C. Seeman, *Annu. Rev. Biophys. Biomol. Struct.*, 1998, **27**, 225–248.
3 N. C. Seeman, *Q. Rev. Biophys.*, 2005, **38**, 363–371.
4 N. C. Seeman, *Trends Biochem. Sci.*, 2005, **30**, 119–125.
5 B. Ding and N. C. Seeman, *Science*, 2006, **314**, 1583–1585.
6 J. H. Chen and N. C. Seeman, *Nature*, 1991, **350**, 631–633.
7 Y. Zhang and N. C. Seeman, *J. Am. Chem. Soc.*, 1994, **116**, 1661–1669.
8 W. M. Shih, J. D. Quispe and G. F. Joyce, *Nature*, 2004, **427**, 618–621.
9 R. P. Goodman, A. T. Schaap, C. F. Tardin, C. M. Erben, R. M. Berry, C. F. Schmidt and A. J. Turberfield, *Science*, 2005, **310**, 1661–1665.
10 C. M. Erben, R. P. Goodman and A. J. Turberfield, *J. Am. Chem. Soc.*, 2007, **6**, 6992–6993.
11 F. A. Aldaye and H. F. Sleiman, *J. Am. Chem. Soc.*, 2007, **129**, 13376–13377.
12 A. Y. Koyfman, S. N. Magonov and N. O. Reich, *Langmuir*, 2009, **25**, 1091–1096.
13 U. Majumder, A. Rangnekar, K. V. Gothelf, J. H. Reif and T. H. LaBean, *J. Am. Chem. Soc.*, 2011, **133**, 3843–3845.
14 J. Zheng, J. J. Birktoft, Y. Chen, T. Wang, R. Sha, P. E. Constantinou, S. L. Ginell, C. Mao and N. C. Seeman, *Nature*, 2009, **461**, 74–77.
15 A. Rangnekar, K. V. Gothelf and T. H. LaBean, *Nanotechnology*, 2011, **22**, 235601.
16 T. H. LaBean, H. Yan, J. Kopatsch, F. Liu, E. Winfree, J. H. Reif and N. C. Seeman, *J. Am. Chem. Soc.*, 2000, **122**, 1848–1860.
17 D. Reishus, B. Shaw, Y. Brun, N. Chelyapov and L. Adleman, *J. Am. Chem. Soc.*, 2005, **127**, 17590–11759.
18 J. Lee, S. Kim, J. Kim, C.-W. Lee, Y. Roh and S. H. Park, *Angew. Chem., Int. Ed.*, 2011, **50**, 9145–9149.
19 X. Sun, H. S. Ko, C. Zhang, A. E. Ribbe and C. J. Mao, *J. Am. Chem. Soc.*, 2009, **131**, 13248.
20 S. Hamada and S. Murata, *Angew. Chem., Int. Ed.*, 2009, **48**, 6820.
21 B. Kim, R. Amin, J. Lee, K. Yun and S. H. Park, *Chem. Commun.*, 2011, **47**, 11053.
22 X. Sun, S. Hyeon Ko, C. Zhang, A. E. Ribbe and C. Mao, *J. Am. Chem. Soc.*, 2009, **131**, 13248–13249.
23 J. Lee, S. Hamada, S. U. Hwang, R. Amin, J. Son, S. R. Dugasani, S. Murata and S. H. Park, *Sci. Rep.*, 2013, **3**, 2115.
24 A. Y. Koyfman, S. N. Magonov and N. O. Reich, *Langmuir*, 2009, **25**, 1091.
25 E. Winfree, F. Liu, L. A. Wenzler and N. C. Seeman, *Nature*, 1998, **394**, 539–544.
26 J. Lee, R. Amin, B. Kim, S. Kim, C. W. Lee, J. M. Kim, T. H. LaBean and S. H. Park, *Soft Matter*, 2012, **8**, 44–47.
27 T. J. Fu, *Biochemistry*, 1993, **32**, 3211–3220.
28 H. Yan, S. H. Park, G. Finkelstein, J. H. Reif and T. H. LaBean, *Science*, 2003, **301**(5641), 1882–1884.
29 Y. He, Y. Chen, H. P. Liu, A. E. Ribbe and C. D. Mao, *J. Am. Chem. Soc.*, 2005, **127**, 12202–12203.